



UNIVERSITY OF LEEDS

This is a repository copy of *Tunable terahertz band-stop filter using strongly coupled split ring resonators integrated with on-chip waveguide*.

White Rose Research Online URL for this paper:  
<http://eprints.whiterose.ac.uk/170228/>

Version: Accepted Version

---

**Article:**

Parker-Jervis, RS, Park, S [orcid.org/0000-0001-8606-191X](https://orcid.org/0000-0001-8606-191X) and Cunningham, JE [orcid.org/0000-0002-1805-9743](https://orcid.org/0000-0002-1805-9743) (2021) Tunable terahertz band-stop filter using strongly coupled split ring resonators integrated with on-chip waveguide. *Journal of Applied Physics*, 129 (5). 053101. ISSN 0021-8979

<https://doi.org/10.1063/5.0040054>

---

This article may be downloaded for personal use only. Any other use requires prior permission of the author and AIP Publishing. This article appeared in *J. Appl. Phys.* 129, 053101 (2021) and may be found at <https://doi.org/10.1063/5.0040054>

**Reuse**

Items deposited in White Rose Research Online are protected by copyright, with all rights reserved unless indicated otherwise. They may be downloaded and/or printed for private study, or other acts as permitted by national copyright laws. The publisher or other rights holders may allow further reproduction and re-use of the full text version. This is indicated by the licence information on the White Rose Research Online record for the item.

**Takedown**

If you consider content in White Rose Research Online to be in breach of UK law, please notify us by emailing [eprints@whiterose.ac.uk](mailto:eprints@whiterose.ac.uk) including the URL of the record and the reason for the withdrawal request.



[eprints@whiterose.ac.uk](mailto:eprints@whiterose.ac.uk)  
<https://eprints.whiterose.ac.uk/>

# Tuneable Terahertz Band-Stop Filter using Strongly Coupled Split Ring Resonators Integrated with On-Chip Waveguide

Rowan S. Parker-Jervis, Sae June Park\*, John E. Cunningham

School of Electronic and Electrical Engineering, University of Leeds, Woodhouse Lane, Leeds, LS2 9JT, United Kingdom.

\* Correspondence:  
s.park@leeds.ac.uk

**Keywords:** On-chip terahertz spectroscopy, split-ring resonator, band-stop filter, waveguide, Goubau line, strong coupling, Rabi splitting.

We have used finite-element methods to design and simulate a tuneable terahertz frequency range band-stop filter based on coupled split-ring resonators integrated into planar Goubau-line waveguide. Two split-ring resonators with different geometrical lengths and gap widths were designed to resonate at the same frequency. When the two resonators were coupled, resonance splitting was observed in the transmission spectra controlled by the distance between them. The electric field distribution and surface current modes in the coupled resonators were used to identify the origin of the resonance modes. In order to dynamically tune the coupled resonance frequencies, a cantilevered microelectromechanical scheme is proposed, in which the radius of curvature of one split-ring resonator is adjusted with respect to a fixed second split-ring resonator. The coupling strength of the coupled resonators was investigated as a function of the relative separation of the resonators revealing a dispersion relation which shows anti-crossing of the coupled resonances as the cantilever bends.

## INTRODUCTION

On-chip terahertz time-domain spectroscopy (THz-TDS) has been used previously to investigate the THz frequency range response of polycrystalline materials,<sup>1</sup> liquids<sup>2</sup> and even of low-dimensional systems.<sup>3</sup> Such on-chip THz spectroscopies enhance interaction of THz radiation with the target material compared to free-space measurements,<sup>4</sup> relying on the injection and propagation of THz pulses through a planar waveguide.<sup>3,5</sup> These pulses can be coupled to materials in close proximity either by the evanescent THz electric field,<sup>6</sup> or by the direct injection and extraction of the THz currents.<sup>5</sup> It has been demonstrated that frequency components within such pulses can be filtered through integration of resonant stub filters into the waveguide, for example.<sup>7</sup>

Wireless communication traffic has drastically increased in recent years along with a demand for higher data rates.<sup>8</sup> This increase in traffic in turn increases the demand for a greater bandwidth of available frequencies, which is now pushing into the THz range for some systems.<sup>9</sup> For practical THz communication devices to become a reality there is a compelling need to understand the behaviour of THz waves in on-chip systems, so permitting the development of components that can manipulate them.<sup>10</sup> Filtering of THz waves has been widely demonstrated in free-space THz systems,<sup>11</sup> though it has also been shown in on-chip devices by integrating split-ring resonators (SRRs),<sup>12,13</sup> following earlier demonstrations of the use of stub filters,<sup>14</sup> for example.

SRRs are particularly promising components for the manipulation of THz waves propagating in a waveguide; they typically comprise metal resonators<sup>15</sup> acting as an inductive-capacitive (LC) circuit<sup>16</sup> able to resonate with electromagnetic waves over a specific range of frequencies controlled by their geometry. The geometrical parameters of an SRR (the width of the gap and the length of the ring) determine the resonant frequency.<sup>17</sup> Liu *et al.* demonstrated that two vertically aligned and coupled SRRs can produce a transmittance spectra containing multiple discrete resonance modes when the SRRs are rotated at varying angles to one another.<sup>18</sup> Furthermore, when two or more THz resonators are in close proximity, they experience near-field coupling, which modifies their response.<sup>19</sup> It has also been shown that the response of a THz SRR can be adjusted by making a microelectromechanical systems (MEMS) cantilever from one arm of the SRR,<sup>20</sup> whose position and resonant response can then be adjusted using voltage. Tuneability of the resonances of the SRR was demonstrated in the frequency range of 200 – 450 GHz for LC resonance and 700 – 1000 GHz for dipole resonance by changing the cantilever position.

Here, we propose to integrate two coupled THz SRRs in close proximity with an on-chip Goubau-line waveguide, to form a coupled system whose frequency response can be controlled within a MEMS approach. We first investigate resonance splitting of the coupled two-SRR system as a function of their proximity to one another. Then, by introducing a cantilever to the outer ring, we explore the effect of the curvature radius of the cantilever on the propagating radiation, demonstrating that the system acts as a tuneable band-stop filter. The coupling strength between the resonators is extracted with respect to the interaction between the two SRRs. A dispersion relation obtained by varying the curvature radius of the cantilever shows an anti-crossing of the coupled resonances.

## SIMULATION RESULTS AND DISCUSSIONS

The two SRRs coupled to a PGL waveguide were simulated using ANSYS High-Frequency Structure Simulator (HFSS), allowing the system's frequency-dependent transmission and resonant frequencies to be calculated. Each SRR geometry was first tuned to give a resonant frequency at 272.5 GHz, chosen to lie in an easily accessible region of frequency for on-chip THz TDS.<sup>1</sup> **Figure 1(a)** shows the system of two coupled SRRs, one inside the another; we refer to the two SRRs as the “inner-SRR” and “outer-SRR” accordingly. The edge of the outer SRR was placed 1.5  $\mu\text{m}$  away from a 1 mm long 5  $\mu\text{m}$  wide PGL waveguide, to which it is then coupled by evanescent electric field extending from the waveguide. Other geometrical parameters of the two SRRs are shown in **Fig. 1(b)**, with the corresponding dimensions given in **Table 1**.

Two-port S-parameter simulations were carried out to obtain the transmission spectra ( $S_{21}$ ) for the two SRRs using HFSS. The THz signals were generated at a wave-port and were then directly coupled to the PGL waveguide.<sup>1</sup> A radiation boundary was assigned to the air box (1000 $\times$ 250 $\times$ 250  $\mu\text{m}$ ) containing the device structures to mimic continued propagation beyond the boundary plane. It has been previously confirmed that this configuration produces a PGL mode propagating along the PGL, suitable for characterisation of a series of coupled SRRs.<sup>21</sup> Our simulations were carried out for a loss-free<sup>22</sup> gallium arsenide substrate with permittivity of 12.9, suitable for developing MEMS based cantilever devices.<sup>23</sup> We note that a loss tangent of gallium arsenide substrate is negligibly small, yielding 0.0006 at 300 GHz.<sup>24</sup> **Figure 1(c)** shows the resonances observed for each SRR when the other is not present, with both centred on 272.5 GHz. The inner SRR has a higher quality factor ( $Q = 60.43$ ) compared to the outer SRR ( $Q = 9.44$ ) as a result of the radiative damping factor increasing with  $l_x$ .<sup>25</sup> We note that

the outer SRR show a greater depth of resonance since its edge was closer to the Goubau line compared to the inner SRR.

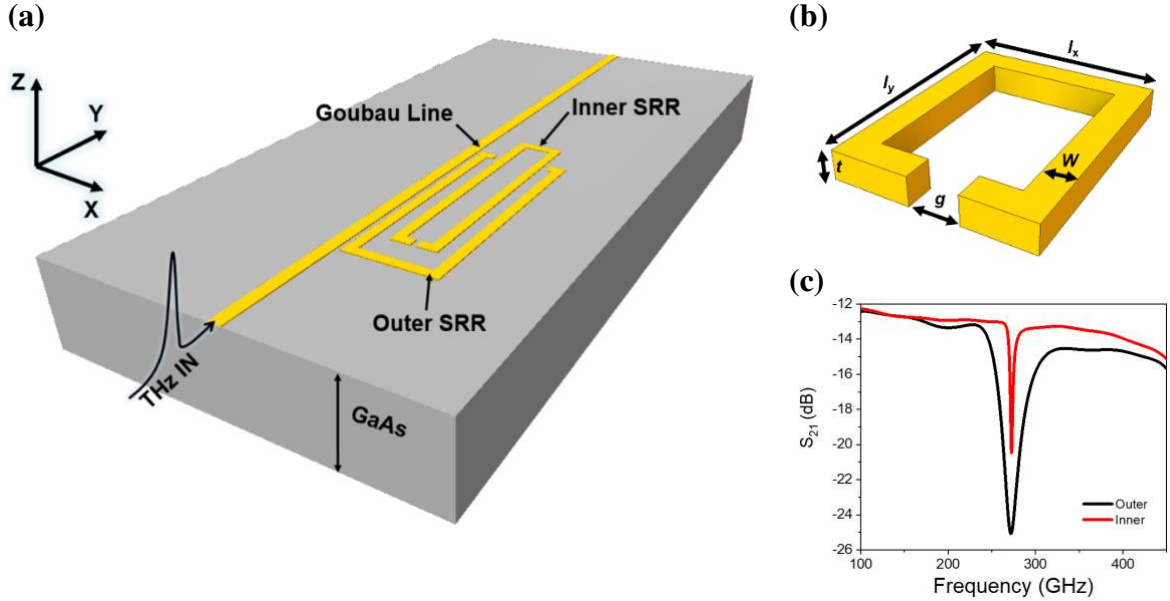


**FIG. 1.** (a) Schematic of the simulated geometry. Two SRRs (inner and outer) are located next to a PGL on top of a GaAs substrate. (b) An example of an SRR pattern labelled with its geometrical factors,  $l_x$ ,  $l_y$ ,  $t$ ,  $g$  and  $w$ . The values for each SRR are given in **Table 1**. (c) The transmission parameter  $S_{21}$  calculated for each SRR without the other present.

**TABLE 1** | Geometrical parameters of SRRs used in this work.

SRR	$f$ (GHz)	$l_x$ ( $\mu\text{m}$ )	$l_y$ ( $\mu\text{m}$ )	$w$ ( $\mu\text{m}$ )	$g$ ( $\mu\text{m}$ )	$t$ (nm)
Inner	272.5	18	97	4	2	150
Outer	272.5	36	94	4	23	150

In order to explore the coupling between the two SRRs, the system was then simulated with both rings present for a variable 5 to 160  $\mu\text{m}$  relative distance ( $d$ ) between the rings. **Figures 2(a)** and **2(b)** illustrate the two SRRs at separations of 140  $\mu\text{m}$  (uncoupled) and 10  $\mu\text{m}$  (coupled), respectively. **Figure 2(c)** shows the separated  $S_{21}$  transmission parameters highlighting the single resonance at  $d = 140 \mu\text{m}$  (red solid line), with a full-width at half-maximum (FWHM) of 18.6 GHz, a Q-factor of 14.6 and an extinction ratio of -16.4 dB, and the full separation of this resonance into two distinct resonances at  $d = 10 \mu\text{m}$  (black solid line), with FWHMs of 7 GHz and 15.1 GHz, Q-factors of 35.88 and 22, and an extinction ratio of -15 dB and -6.1 dB for lower frequency resonance and higher frequency resonance, respectively. We note that a simple resonance overlap occurs when  $d = 140 \mu\text{m}$ , hence the Q-factor is mainly dominated by the outer SRR which has a relatively low Q-factor compared to the inner SRR. When  $d = 10 \mu\text{m}$ , however, the Q-factors are determined by resonance mode hybridisation between the outer (low Q-factor) and the inner (high Q-factor) SRRs causing an increase in the Q-factor compared to when  $d = 140 \mu\text{m}$ . We also note that the depth of the resonances when  $d = 10 \mu\text{m}$  could be enhanced by adding a number of the coupled SRRs along the THz wave propagation path. **Figure 2(d)** shows a colour-scale plot of all the  $S_{21}$  parameters across the range of values for  $d$ . When  $d$  is increased to greater than 100  $\mu\text{m}$ , only a single resonance is visible since they are then fully uncoupled and so act independently of one another. The SRRs then resonate at the same frequency producing one resonance.<sup>26</sup> By situating two SRRs in close

proximity they experience near-field capacitive coupling however,<sup>19</sup> which causes resonant splitting for relative distances of less than 100  $\mu\text{m}$  into two modes. **Figure 2(e)** shows the electrical field distribution and circulating surface current modes for the uncoupled inner and outer SRRs when  $d = 140 \mu\text{m}$ . **Figure 2(f)** presents the electric field distribution and surface current directions of the coupled SRRs when  $d = 10 \mu\text{m}$ . The coupled system is simulated at the two resonant frequencies identified in **Fig. 2(c)**, showing that the surface current directions in the coupled SRRs are in phase at 221 GHz, and out of phase at 332 GHz.

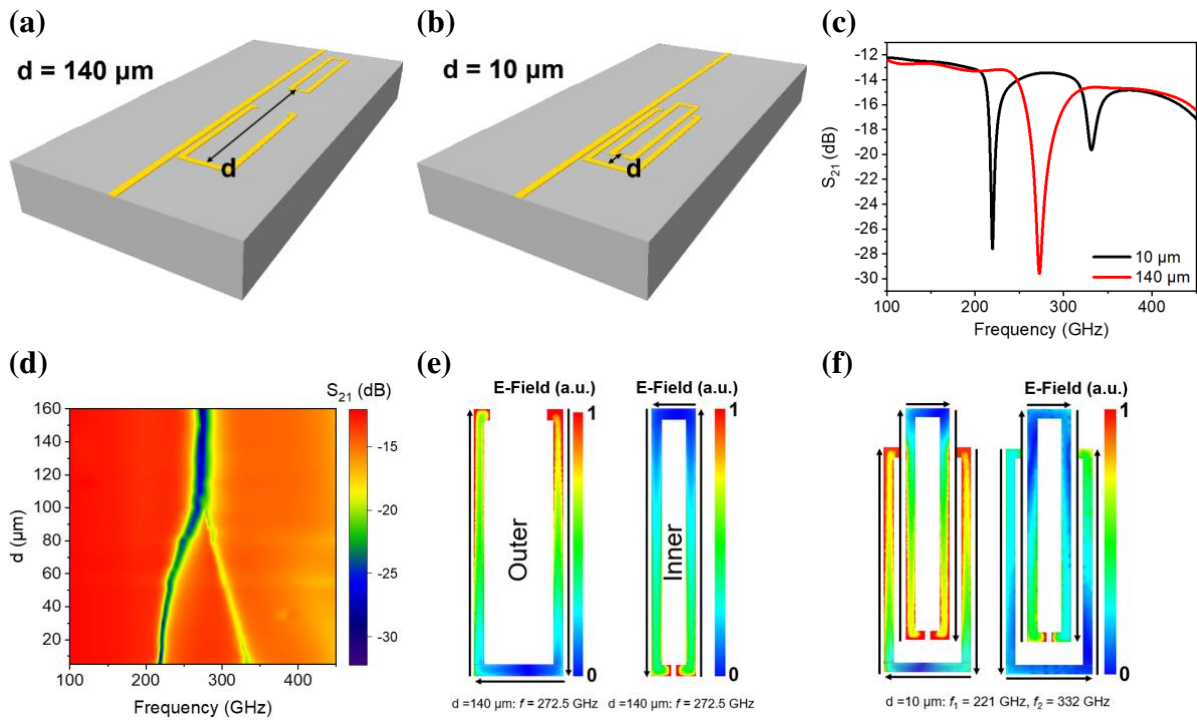


**FIG. 2.** (a) The system when the two SRRs are uncoupled at a relative distance  $d$  of 140  $\mu\text{m}$ . (b) The system when the two SRRs are coupled together and have a relative distance  $d$  of 10  $\mu\text{m}$ . (c)  $S_{21}$  Transmission parameters calculated for relative distance  $d = 10 \mu\text{m}$  and 140  $\mu\text{m}$ . (d)  $S_{21}$  parameter for relative distances from 160  $\mu\text{m}$  to 5  $\mu\text{m}$  demonstrating the formation of a split resonance at a relative distance of  $\sim 100 \mu\text{m}$ . (e) A colour scale plot of field magnitude (plotted in arbitrary units) and the surface current direction (black arrows) for the outer and inner SRR when separated,  $d = 140 \mu\text{m}$ , at the frequency of 272.5 GHz. (f) A colour scale plot of field magnitude (plotted in arbitrary units) and the surface current direction (black arrows) for the coupled SRRs, relative distance  $d = 10 \mu\text{m}$ , at the two resonant frequencies, 221 GHz and 332 GHz.

A cantilever comprising the arms of the outer SRR was then introduced to actively control the coupling between the two SRRs. It altered the geometry of one SRR by bending it away from the other SRR, so also controlling the coupling between the two SRRs. We mimic a MEMS cantilever for actuation of the cantilever.<sup>13</sup> **Figure 3(a)** illustrates the method used, in which we simulate the outer SRR bending away from the substrate while the position of the inner SRR remains fixed. We varied curvature of the outer SRR so that it adopted the progressive range of radii depicted in **Figure 3(a)**. The range of radii values simulated was based on experimental results<sup>20</sup> that show a minimum value of bend radius of 45  $\mu\text{m}$  can be achieved for a 71- $\mu\text{m}$ -long moving GaAs MEMS cantilever, the ratio between the radius and the length thus being 0.63. **Figure 3(b)** shows our SRR outer cantilever which was carved out of the smallest

of the rings shown in **Figure 3(a)**. The radius of its curvature was set at a minimum simulated value of  $57 \mu\text{m}$  to keep the same ratio (of 0.63) between the radius and the length of the cantilever as demonstrated in experiments.<sup>20</sup> **Figure 3(c)** presents the electric field distribution and surface current for the system when  $d = 10 \mu\text{m}$  and with the cantilever  $r$  is set at three different values, 0.1 m, 0.01 m, and  $57 \mu\text{m}$ . The figure shows that the field amplitude in the outer SRR decreases as the radius is decreased whilst it increases for the inner SRR. This is to be expected for as it bends away it is then increasingly difficult for the incident THz wave to couple with the outer SRR.

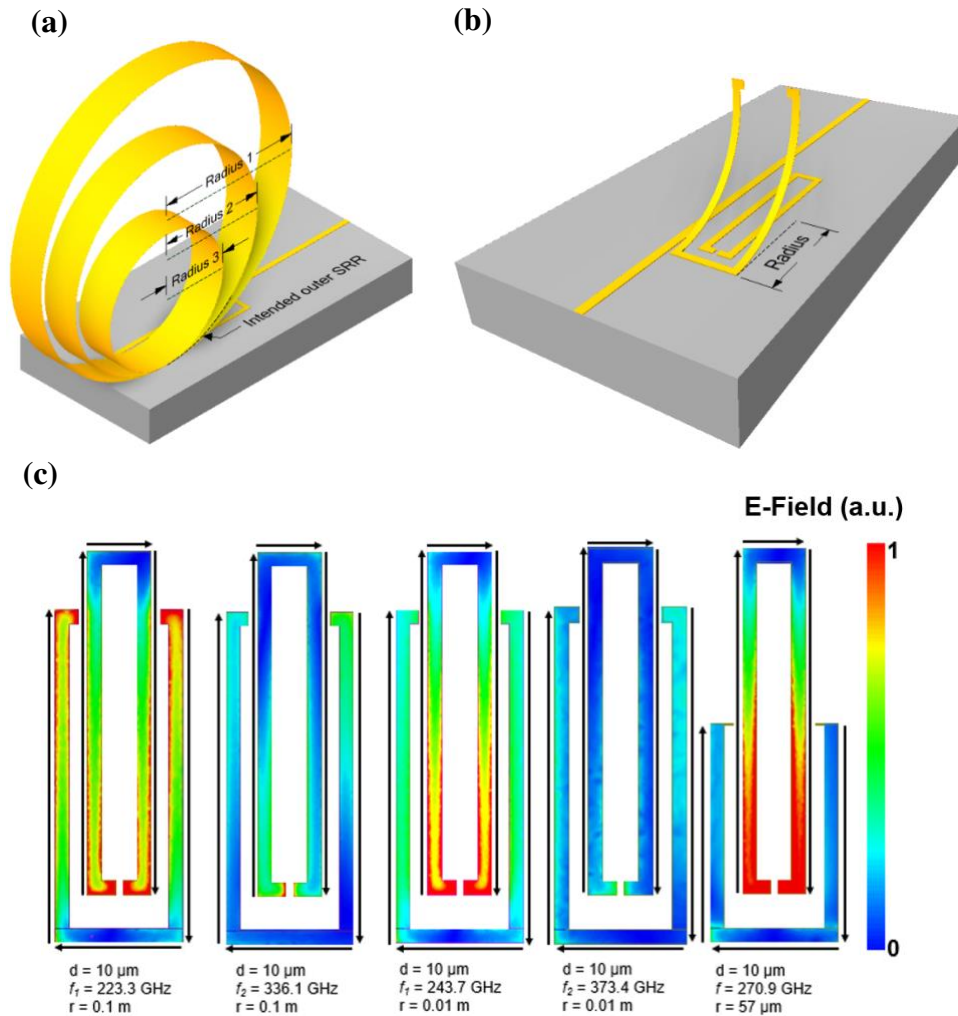


**FIG. 3.** (a) Cylinders showing how the cantilever bend was varied by changing its radius. (b) The outer SRR displaying curvature with a radius of  $57 \mu\text{m}$ , by which point it can no longer tune the signal. (c) Five colour scale plots of the field magnitude (plotted in arbitrary units) and surface current direction at the resonant frequencies when  $d = 10 \mu\text{m}$  and the resonator radius is set at 0.1 m, 0.01 m, and  $57 \mu\text{m}$ . The black arrows represent the direction of the surface current.

The cantilevered system was simulated at both a relative distance of  $10 \mu\text{m}$  and  $140 \mu\text{m}$  to show the response for cases when the SRRs were strongly coupled and completely uncoupled. In the case of  $10 \mu\text{m}$ , the SRRs were coupled and the cantilever controlled the coupling efficiency as well tuning the frequency. This contrasts with the  $140 \mu\text{m}$  case, where the SRRs were completely uncoupled and so the action of the cantilever purely tunes the resonant frequency of the outer SRR. **Figure 4(a)** presents the  $S_{21}$  parameters of the SRRs when  $d$  is  $10 \mu\text{m}$  and  $r$  was set at 0.1 m, 0.01 m and  $57 \mu\text{m}$ . When the radius is 0.1 m two resonances are visible owing

to the capacitive coupling between two SRRs; as the radius decreases the upper frequency branch disappears while the lower frequency branch is left at 270 GHz. **Figure 4(b)** presents a 2D colour plot scale of the case  $d = 10 \mu\text{m}$  when the SRRs are strongly coupled. As the outer SRR cantilever bends the split resonances blue-shift. The second resonance is no longer visible again when the cantilever has a radius less than 0.001 m, therefore demonstrating the system's ability to tune the resonating modes. We note that the operating frequency can be tuned in the range of 220 – 250 GHz and 335 – 427 GHz for the lower frequency resonance and higher frequency resonance, respectively. **Figure 4(c)** shows the  $S_{21}$  parameters of the SRRs when  $d$  is 140  $\mu\text{m}$  for  $r = 0.1, 0.01$  and  $5.7 \times 10^{-5}$  m. When  $r = 0.1$  m only a single resonance is observed, but when  $r$  drops to 0.01 m, a second resonance can also be observed at a frequency of 272.5 GHz. This is attributed to the inner SRR which does not have a cantilever then being uncoupled to the outer SRR. **Figure 4(d)** illustrates this more clearly by showing the  $S_{21}$  parameters with the initial single resonance visibly blue-shifted as the radius is decreased, with a sharp resonance remaining at the initial frequency. For values of radius of less than 0.001 m the tuned resonance is no longer visible owing to the outer SRR bending too far away to interact appreciably with incident THz wave.

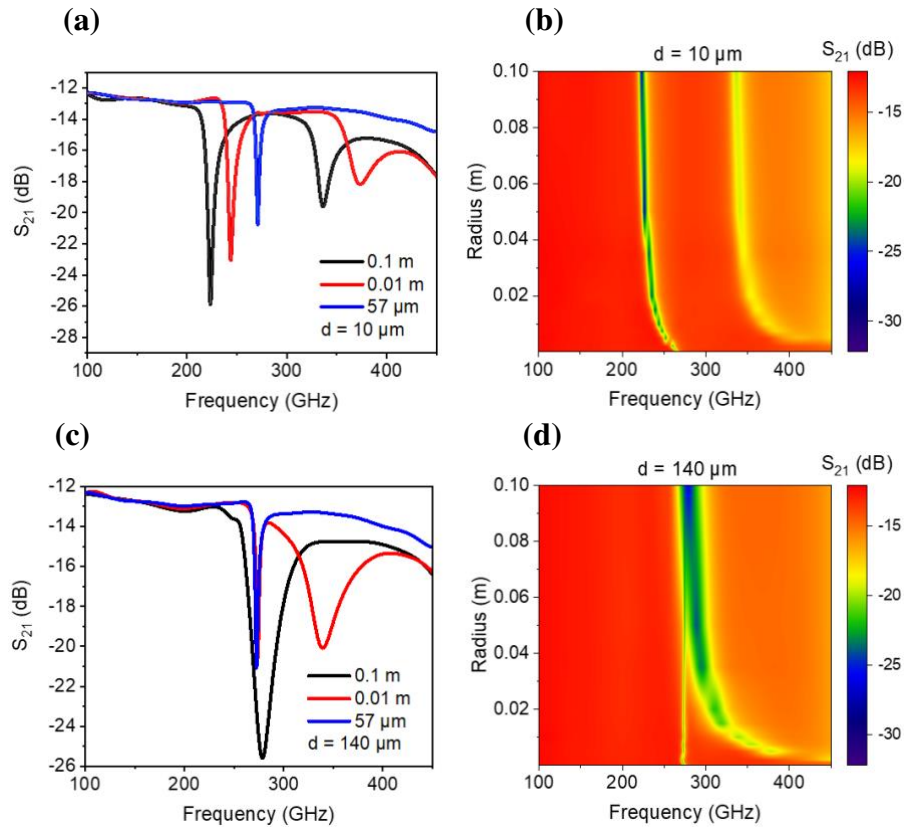


**FIG. 4.** (a) Three  $S_{21}$  Transmission parameters calculated for radii 0.1 m, 0.01 m and 57  $\mu\text{m}$  when  $d = 10 \mu\text{m}$ . (b) The  $S_{21}$  parameters for the integrated outer SRR (cantilever) and inner SRR, separated by a distance  $d = 10 \mu\text{m}$ , as a function of radius. (c) Three  $S_{21}$  Transmission parameters calculated for radii 0.1 m, 0.01 m and 57  $\mu\text{m}$  when  $d = 140 \mu\text{m}$ . (d) The  $S_{21}$  parameters for the integrated outer SRR (cantilever) and inner SRR, separated by a distance  $d = 140 \mu\text{m}$ , as a function of radius.

To describe the coupling behaviour in our geometry more quantitatively, we calculate the coupling strength ( $V_A$ ) of the coupled SRRs as a function of  $d$ . The resonance splitting can be interpreted by obtaining the solution of a coupled oscillator model for  $E_{\text{SRR},o} = E_{\text{SRR},i}$ , where  $E_{\text{SRR},o}$  and  $E_{\text{SRR},i}$  are the resonant energy of outer SRR and inner SRR, respectively. The Rabi

splitting energy ( $\hbar\Omega_{\text{Rabi}}$ ) caused by the SRRs coupling can be described by Equation (1), where  $\hbar$  is the reduced Planck's constant,  $\Gamma_{\text{SRR,o}}$  and  $\Gamma_{\text{SRR,i}}$  are the half-width at half-maximum of the resonance of outer SRR and inner SRR, respectively.<sup>27,28</sup>

$$\hbar\Omega_{\text{Rabi}} = 2\sqrt{V_A^2 - \left(\frac{1}{4}\right)(\hbar\Gamma_{\text{SRR,o}} - \hbar\Gamma_{\text{SRR,i}})^2} \quad (1)$$

From Equation (1),  $V_A$  was extracted as a function of  $d$  as shown in **Fig. 5(a)**. It is noteworthy that the coupling occurs when  $d < 100 \mu\text{m}$  and  $V_A$  gradually increases up to 0.24 meV as  $d$  decreases to 10  $\mu\text{m}$ . Here, strong coupling regime can be defined where  $V_A > \sqrt{((\hbar\Gamma_{\text{SRR,o}})^2 + (\hbar\Gamma_{\text{SRR,i}})^2)/2}$ ,<sup>27</sup> which leads to  $V_A > 0.057 \text{ meV}$  (red solid line). We note that the strong coupling is required to achieve frequency tuning of split resonances. The dispersion curve presented in **Fig. 5(b)** shows the  $S_{21}$  parameters of the SRRs as a function of  $f_{\text{SRR,o}}$ .  $f_{\text{SRR,o}}$  was tuned by changing the bend of the cantilever of the outer SRR when  $d = 10 \mu\text{m}$ . Black and green dashed lines show simulations of the uncoupled outer and inner SRR, respectively, converging on one another as  $f_{\text{SRR,o}}$  approaches to  $f_{\text{SRR,i}}$ . On the other hand, blue dashed lines show the case for the coupled SRRs for which an anti-crossing emerges compared to the uncoupled case as  $f_{\text{SRR,o}}$  approaches to  $f_{\text{SRR,i}}$ . We again obtained  $V_A$  of 0.24 meV when  $f_{\text{SRR,o}} = f_{\text{SRR,i}}$  ( $r = 0.1 \text{ m}$ ) in the coupled case. We can thus expect to be able to control the anti-crossing behaviour in our device with applied cantilever voltage and have shown that this behaviour needs to be taken into consideration in the overall design of such systems.

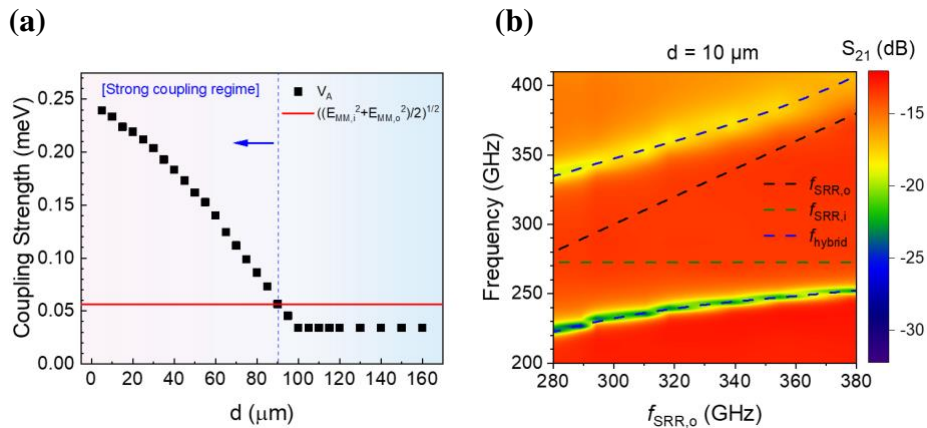


**FIG. 5.** (a) Coupling strength as a function of  $d$ . The Red solid line represents the criterion for the strong coupling regime ( $V_A = 0.057 \text{ meV}$ ). (b) A dispersion curve showing the  $S_{21}$  parameters of the SRRs as a function of  $f_{\text{SRR,o}}$ .

## CONCLUSIONS

We have proposed a new on-chip device capable of frequency filtering in the THz range (200 – 400GHz) formed from two interacting SRRs. By situating one SRR inside the other they experience strong capacitive coupling causing the resonant frequency to split into two. Splitting of the resonant frequency with respect to the relative distance of the two SRRs was investigated thus allowing us to determine their coupling strength. We demonstrated that forming a cantilever from the outer SRR allows control of the degree of capacitive coupling between the two, and thus the resonant frequencies. Anti-crossing behaviour was observed in the dispersion curve, confirming that our system can achieve strong coupling between the SRRs dependent on the cantilever position, so confirming that such effects need to be considered in overall system design and optimisation of on-chip filters using coupled THz SRRs.

## **Author Contributions**

Conceptualization, S.J.P.; methodology, S.J.P., R. P.-J. and J.E.C.; validation, S.J.P., R. P.-J. and J.E.C.; formal analysis, S.J.P., R. P.-J. and J.E.C.; writing—original draft preparation, S.J.P., R. P.-J. and J.E.C.; writing—review and editing, S.J.P., R. P.-J. and J.E.C.; All authors have read and agreed to the published version of the manuscript.

## **Funding**

This research was funded by Engineering and Physical Sciences Research Council (EPSRC), grant numbers EP/R00501X/1 and EP/P021859/1.

## **Data Availability Statement**

The data associated with this paper is available from University of Leeds at <https://doi.org/10.5518/941>.

## **Conflict of Interest**

*The authors declare that the research was conducted in the absence of any commercial or financial relationships that could be construed as a potential conflict of interest.*

## REFERENCES

- <sup>1</sup> C. Russell, C.D. Wood, A.D. Burnett, L. Li, E.H. Linfield, A.G. Davies, and J.E. Cunningham, *Lab Chip* **13**, 4065 (2013).
- <sup>2</sup> M. Swithenbank, A.D. Burnett, C. Russell, L.H. Li, A.G. Davies, E.H. Linfield, J.E. Cunningham, and C.D. Wood, *Anal. Chem.* **89**, 7981 (2017).
- <sup>3</sup> C.D. Wood, D. Mistry, L.H. Li, J.E. Cunningham, E.H. Linfield, and A.G. Davies, *Rev. Sci. Instrum.* **84**, (2013).
- <sup>4</sup> N. Peters, M. Rosamond, L. Li, E.H. Linfield, A.G. Davies, M. Ali, B.J. Hickey, and J. Cunningham, *Appl. Phys. Lett.* **112**, (2018).
- <sup>5</sup> D.R. Grischkowsky, *IEEE J. Sel. Top. Quantum Electron.* **6**, 1122 (2000).
- <sup>6</sup> J. Wu, A.S. Mayorov, C.D. Wood, D. Mistry, L. Li, W. Muchenje, M.C. Rosamond, L. Chen, E.H. Linfield, A.G. Davies, and J.E. Cunningham, *Sci. Rep.* **5**, 1 (2015).
- <sup>7</sup> J. Cunningham, C. Wood, A.G. Davies, I. Hunter, E.H. Linfield, and H.E. Beere, *Appl. Phys. Lett.* **86**, 1 (2005).
- <sup>8</sup> I.F. Akyildiz, J.M. Jornet, and C. Han, *Phys. Commun.* **12**, 16 (2014).
- <sup>9</sup> J. Federici and L. Moeller, *J. Appl. Phys.* **107**, (2010).
- <sup>10</sup> A.S. Meijer, G. Berden, D.D. Arslanov, M. Ozerov, R.T. Jongma, and W.J. Van Der Zande, *Nat. Photonics* **10**, 740 (2016).
- <sup>11</sup> W. Junlin, Z. Binzhen, W. Xin, and D. Junping, *Opt. Mater. Express* **7**, 1656 (2017).
- <sup>12</sup> Z. Han, K. Kohno, H. Fujita, K. Hirakawa, and H. Toshiyoshi, *IEEE J. Sel. Top. Quantum Electron.* **21**, 114 (2015).
- <sup>13</sup> Y.-S. Lin, F. Ma, and C. Lee, *Opt. Lett.* **38**, 3126 (2013).
- <sup>14</sup> J. Cunningham, C. Wood, A.G. Davies, C.K. Tiang, P. Tosch, D.A. Evans, E.H. Linfield, I.C. Hunter, and M. Missous, *Appl. Phys. Lett.* **88**, 86 (2006).
- <sup>15</sup> H.T. Chen, W.J. Padilla, J.M.O. Zide, A.C. Gossard, A.J. Taylor, and R.D. Averitt, *Nature* **444**, 597 (2006).
- <sup>16</sup> J.D. Baena, J. Bonache, F. Martín, R.M. Sillero, F. Falcone, T. Lopetegui, M.A.G. Laso, J. García-García, I. Gil, M.F. Portillo, and M. Sorolla, *IEEE Trans. Microw. Theory Tech.* **53**, 1451 (2005).
- <sup>17</sup> H. Guo, N. Liu, L. Fu, H. Schweizer, S. Kaiser, and H. Giessen, *Phys. Status Solidi Basic Res.* **244**, 1256 (2007).
- <sup>18</sup> H. Liu, Y.M. Liu, T. Li, S.M. Wang, S.N. Zhu, and X. Zhang, *Phys. Status Solidi B-Basic Solid State Phys.* **247**, 225 (2010).
- <sup>19</sup> S.J.M. Rao, Y.K. Srivastava, G. Kumar, and D. Roy Chowdhury, *Sci. Rep.* **8**, 1 (2018).

- <sup>20</sup> F. Ma, Y.S. Lin, X. Zhang, and C. Lee, *Light Sci. Appl.* **3**, 1 (2014).
- <sup>21</sup> S.J. Park and J. Cunningham, *Sensors (Switzerland)* **20**, 1 (2020).
- <sup>22</sup> M. Natrella, O. Mitrofanov, R. Mueckstein, C. Graham, C.C. Renaud, and A.J. Seeds, *Opt. Express* **20**, 16023 (2012).
- <sup>23</sup> Z. Yi and X. Liao, *J. Micromechanics Microengineering* **23**, (2013).
- <sup>24</sup> M.N. Afsar and K.J. Button, *IEEE Trans. Microw. Theory Tech.* **31**, 217 (1983).
- <sup>25</sup> C. Novo, D. Gomez, J. Perez-Juste, Z. Zhang, H. Petrova, M. Reismann, P. Mulvaney, and G. V. Hartland, *Phys. Chem. Chem. Phys.* **8**, 3540 (2006).
- <sup>26</sup> D. Roy Chowdhury, R. Singh, A.J. Taylor, H.T. Chen, W. Zhang, and A.K. Azad, *Int. J. Opt.* **2012**, (2012).
- <sup>27</sup> X. Liu, T. Galfsky, Z. Sun, F. Xia, E.C. Lin, Y.H. Lee, S. Kéna-Cohen, and V.M. Menon, *Nat. Photonics* **9**, 30 (2014).
- <sup>28</sup> H.S. Kim, N.Y. Ha, J.Y. Park, S. Lee, D.S. Kim, and Y.H. Ahn, *Nano Lett.* **20**, 6690 (2020).